

# Production of gamma rays by pulsed laser beam Compton scattering off GeV-electrons using a non-planar four-mirror optical cavity

---

T. Akagi<sup>e</sup>, S. Araki<sup>d</sup>, J. Bonis<sup>a</sup>, I. Chaikovska<sup>a\*</sup>, R. Chiche<sup>a</sup>, R. Cizeron<sup>a</sup>, M. Cohen<sup>a</sup>,  
E. Cormier<sup>b</sup>, P. Cornebise<sup>a</sup>, N. Delerue<sup>a</sup>, R. Flaminio<sup>c</sup>, S. Funahashi<sup>d</sup>, D. Jehanno<sup>a</sup>,  
Y. Honda<sup>d</sup>, F. Labaye<sup>a</sup>, M. Lacroix<sup>a</sup>, R. Marie<sup>a</sup>, C. Michel<sup>c</sup>, S. Miyoshi<sup>e</sup>, S. Nagata<sup>e</sup>,  
T. Omori<sup>d</sup>, Y. Peinaud<sup>a</sup>, L. Pinard<sup>c</sup>, H. Shimizu<sup>d</sup>, V. Soskov<sup>a</sup>, T. Takahashi<sup>e</sup>,  
R. Tanaka<sup>e</sup>, T. Terunuma<sup>d</sup>, J. Urakawa<sup>d</sup>, A. Variola<sup>a</sup>, F. Zomer<sup>a</sup>.

<sup>a</sup>LAL, CNRS-IN2P3, Université Paris-Sud XI

Centre Scientifique d'Orsay, Bâtiment 200, BP 34, 91898 Orsay cedex, France

<sup>b</sup>CELIA, CNRS, Université de Bordeaux

Domaine du Haut Carré, 43, Rue Pierre Noailles, 33405 Talence, France

<sup>c</sup>LMA, CNRS-IN2P3, Université Claude Bernard Lyon I

Bâtiment Virgo 7, Avenue Pierre de Coubertin, 69622 Villeurbanne cedex, France

<sup>d</sup>ATF, High Energy Accelerator Research Organization (KEK)

1-1 Oho, Tsukuba, 305-0801 Ibaraki, Japan

<sup>e</sup>Hiroshima University

1-3-2 Kagamiyama, Higashi-Hiroshima 739-8511, Japan

E-mail: chaikovs@lal.in2p3.fr

ABSTRACT: As part of the positron source R&D for future  $e^+ - e^-$  colliders and Compton based compact light sources, a high finesse non-planar four-mirror Fabry-Perot cavity has recently been installed at the ATF (KEK, Tsukuba, Japan) [1]. The first measurements of the gamma ray flux produced with a such cavity using a pulsed laser is presented here. We demonstrate the production of a flux of  $2.7 \pm 0.2$  gamma rays per bunch crossing ( $\sim 3 \times 10^6$  gammas per second) during the commissioning.

KEYWORDS: Positrons production; Compton scattering; Fabry-Perot cavity; Gamma rays; ATF.

---

\*Corresponding author.

---

## Contents

<b>1. Introduction</b>	<b>1</b>
<b>2. Experimental setup</b>	<b>2</b>
2.1 Accelerator Test Facility	2
2.2 Fabry-Perot cavity	2
2.3 Calorimeter	3
<b>3. Expected gamma ray flux</b>	<b>4</b>
<b>4. Measurements</b>	<b>5</b>
4.1 Scanning procedure and first data	5
4.2 Example of data	6
4.3 Data analysis	7
4.4 Calibration	10
<b>5. Results</b>	<b>11</b>
<b>6. Conclusion and outlook</b>	<b>15</b>

---

## 1. Introduction

High Energy physics [2, 3, 4] as well as applied physics [5, 6, 7, 8] are showing a great interest for intense flux of high energy X-rays and gamma rays.

These gamma or alternatively X-rays can be generated by Compton scattering [9]. To achieve a high flux of high energy photons despite the low cross section of Compton scattering one requires a high average power laser system based on a Fabry-Perot cavity [10] together with a high current electron beam [11]. In this context, a two-mirror Fabry-Perot cavity has already been successfully operated at the Accelerator Test Facility [12] (ATF) of KEK [13, 14].

A solution to produce a high flux of circularly polarized gamma rays is to use a four-mirror Fabry-Perot cavity (FPC) where laser pulses can be stacked to reach a high average power at the interaction point (IP). A prototype of non-planar high finesse four-mirror Fabry-Perot cavity has been installed at the KEK ATF and is described in details in [1]. The optical system has been commissioned during summer 2010 and electron-photon Compton collisions were observed on the first attempt in October 2010. In this paper we present measurements of the gamma ray flux recorded during our commissioning. The data analyzed here were taken before the tragic earthquake which struck Japan in March 2011. Recovery and improvement work is being carried out since but is not covered by this paper.

This paper is organised as follows. Section 2 describes the experimental setup used to produce and measure the gamma rays. Section 3 discusses the gamma ray flux expected with our current setup. Section 4 explains how the data were analyzed. Section 5 presents the gamma ray spectra measured. Finally, the main results and further steps are discussed in section 6.

## 2. Experimental setup

### 2.1 Accelerator Test Facility

A detailed description of the ATF at KEK can be found in [12, 15, 16]. The 1.28 GeV damping ring (DR) has a revolution period of 462 ns and operates at the radio frequency (RF) of 357 MHz (165 RF buckets spaced by 2.8ns). Although a total of up to 3 trains of 10 bunches separated by 5.6 ns can be injected in the ring, most operations run with a single bunch in the train or with a train of up to 10 bunches [17]. Our FPC is installed in one of the straight sections of the damping ring as shown on figure 1. After the collisions the gamma rays, propagating along the electron beam, are extracted through a window before passing through several collimators. They are measured by a gamma detector about 20 m downstream the IP.

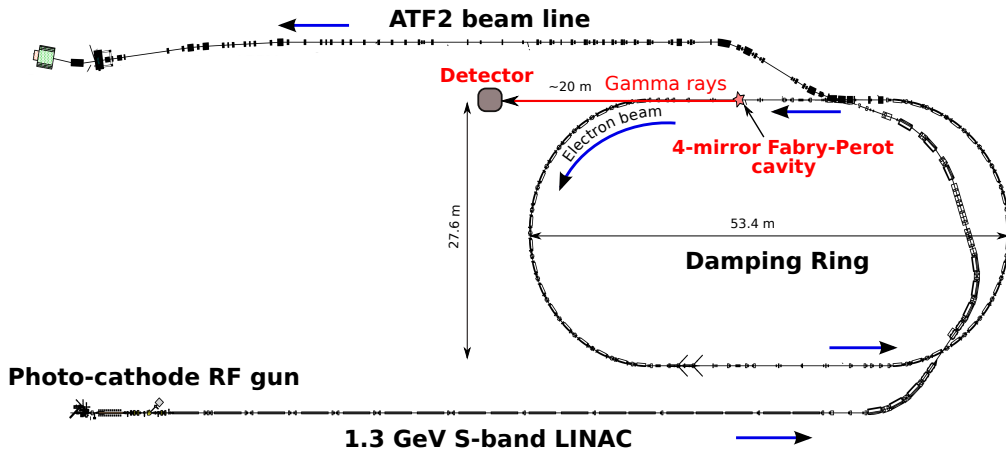


Figure 1: Layout of the Accelerator Test Facility at KEK. The red star indicates the approximate location of the 4-mirror Fabry-Perot cavity described in [1] and used for the measurements presented in this paper. The red arrow indicates the direction of propagation of the gamma rays produced. The grey box indicates the gamma ray detector (adapted from [14]).

The main parameters of the electron beam at the ATF DR are given in the table 1.

### 2.2 Fabry-Perot cavity

The FPC is composed of 2 concave mirrors with a radius of curvature of 0.5 m and two flat mirrors with a non-planar tetrahedron geometry. The mirrors have a very high reflectivity (1 - 1060 ppm for one of them and 1 - 330 ppm for the others) leading to a cavity finesse of the order of 3000

Table 1: ATF DR parameters.

Description	Value
Electron energy, $E_e$	1.28 GeV
Electron bunch population, $N_e$	$\sim 0.5 \times 10^{10}$
Electron bunch length, $\sigma_z/c = \tau_e$	$\sim 20$ ps
Electron beam size, $\sigma_x/\sigma_y$	$\sim 110 / 10 \mu m$
Revolution period, $T_0$	462 ns
Emittance, $\gamma\epsilon_{x/y}$	$5 \times 10^{-6} / 3 \times 10^{-8}$ m·rad

(corresponding to a passive power enhancement of about 1000). A round trip time of 5.6 ns in the FPC is set to match half the RF frequency of the ATF DR at 178.5 MHz.

A passively mode-locked oscillator is amplified in a microstructured active fiber and further injected in the FPC. An all-digital double feedback system is used to lock the cavity on the ATF clock and to ensure that the laser pulses are properly stacked with interferometric accuracy.

The FPC is mounted on an optical table which is itself mounted on movers that allow to control precisely the vertical position of the FPC with respect to that of the laser beam.

Table 2 summarises the main parameters of the system and more details on the experimental apparatus can be found in [1].

Table 2: Parameters of the laser system used during the data taking presented here.

Description	Value
Laser photon energy, $E_{ph}$	1.2 eV ( $\lambda_{ph} = 1032$ nm)
Laser spot size, $\sigma_x/\sigma_y$	26 / 38 $\mu m$
Laser repetition rate, $f_L$	178.5 MHz $\pm$ 4 KHz
Finesse, $F$	$\sim 3000$
Laser pulse length, $\tau_L$	68 ps
Average power stored in FPC, $P_L$	$\sim 160$ W
Crossing angle, $\phi$	8 deg.

As there is an odd number of RF buckets in the DR collisions on a given electron bunch occur only every other turn, at a frequency of 1.08 MHz.

**Data acquisition** The data acquisition relies on several oscilloscopes to acquire information from the FPC and from the calorimeter. The waveforms acquired are timestamped in a database and saved on disk for later analysis. Data from the accelerator such as beam position and charge are also acquired and saved in the database.

### 2.3 Calorimeter

To detect the gamma rays produced by the collisions between the laser photons and the electrons, we use a fast scintillation detector made of barium fluoride ( $BaF_2$ ) coupled with a Photomultiplier

Tube (PMT). Two polished rectangular crystals of  $BaF_2$  with dimensions  $100 \text{ mm} \times 70 \text{ mm} \times 70 \text{ mm}$  are glued to each other and wrapped into an absorbing tape. The 200 mm depth of the  $BaF_2$  calorimeter is nearly 10 radiation lengths, ensuring high detection efficiency [18].

Barium fluoride is commonly used as it has two emission spectra peaks at 220 nm and 310 nm with decay time constants of about 0.8 ns and 630 ns respectively. The decay time of the fast component of  $BaF_2$  allows to resolve two successive pulses of gamma rays generated from the electron bunches spaced by 5.6 ns. To eliminate the slow component of the scintillation an optical filter has been installed in front of the PMT. A fast PMT (Hamamatsu Photonics R3377) with a rise time of 0.7 ns is used. Data acquisition is performed using a LeCroy WS454 oscilloscope (1GS/s, 500 MHz bandwidth).

**GEANT4 simulations** Using Geant4 [19] we simulated the detector to study the development of electromagnetic showers inside the  $BaF_2$  calorimeter.

This allows to perform realistic simulations of high energy gammas passing through the calorimeter. The initial distribution of the gamma rays is obtained by using the beam-beam interaction code CAIN2.40 [20]. Once a gamma ray hits the calorimeter, scintillation light is uniformly emitted along the path of the charged particles produced by the electromagnetic shower. The number of optical photons generated is proportional to the energy loss of the initial gamma rays. The scintillation light then propagates and finally reaches the PMT located at the end of the scintillator.

### 3. Expected gamma ray flux

Using the Compton scattering physical properties it is possible to estimate the expected number of scattered gamma rays in the experiment. Neglecting the divergence of the electron and laser beam at the IP, the luminosity for the Compton collisions is given by equation 3.1 in [21]:

$$\mathcal{L} = N_e N_{ph} f \frac{\cos(\phi/2)}{2\pi} \frac{1}{\sqrt{\sigma_{ye}^2 + \sigma_{yph}^2} \sqrt{(\sigma_{xph}^2 + \sigma_{xe}^2) \cos^2(\phi/2) + (\sigma_{ze}^2 + \sigma_{zph}^2) \sin^2(\phi/2)}}, \quad (3.1)$$

$$\mathcal{F} = \frac{dN_\gamma}{dt} = \sigma_{Compton} \cdot \mathcal{L}, \quad (3.2)$$

where  $N_e$ ,  $N_{ph}$  are the number of the electrons in the bunch and number of the photons in the laser pulse respectively,  $f$  is the repetition frequency,  $\phi$  is the angle of the collisions,  $\sigma_{\vec{r}e}$  and  $\sigma_{\vec{r}ph}$  indicate respectively the RMS sizes of the electron bunch and the laser pulse. Once, the luminosity of the process is defined, the flux of gamma rays is given by formula 3.2, where  $\sigma_{Compton}$  is the total Compton scattering cross section which is determined by the momenta of the incident electron and laser photon [22].

Formulas 3.1 and 3.2 show that the emitted rate is inversely proportional to the transverse electron and laser beam sizes. These formulas shows also that a collision angle reduces the gamma ray flux especially in the case of long electron bunches and laser pulses.

The simulation code CAIN has been used to simulate the Compton scattering process. This code simulates the interaction between one electron bunch and one laser pulse where the Compton cross section is calculated for all the possible polarization states [22] and takes into account the

beam geometry. Using the parameters listed in table 1 and 2 the energy spectrum and expected number of the scattered gamma rays per bunch crossing have been obtained.

As it was mentioned before, in the experiment the scattered gamma rays pass through several collimators before entering the detector. This carries out a gamma energy spectrum selection owing to the energy-angle correlation in Compton scattering. Figure 2 shows the simulated energy spectrum of the gamma rays where the red color refers to the gamma rays transmitted by the collimators and blue color refers to the gamma rays filtered out due to their energy/angle.

The average energy of the gamma rays produced is  $\sim 15$  MeV. However, due to the limited geometrical aperture, the gamma rays below 15 MeV do not reach the detector. The average energy of the gamma rays reaching the detector is therefore 24 MeV. Later, these results are used for the Geant4 simulation and calibration of the calorimeter.

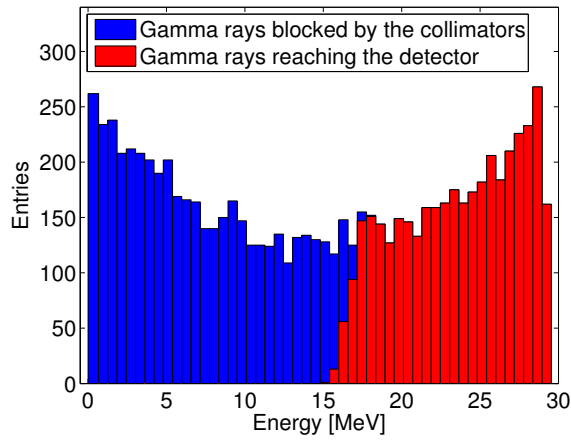


Figure 2: Energy spectrum of the gamma rays. The energies of the gamma rays blocked by the collimators are shown as well as the energies of the gamma rays entering the detector. Only the gamma rays with energies above 15 MeV are accepted by the collimators.

## 4. Measurements

### 4.1 Scanning procedure and first data

The FPC was commissioned in October 2010 and Compton collisions were recorded on the first attempt (26 October). Before data taking we investigated how the intensity of the signal is affected by the position of the laser beam waist with respect to the electron beam position and synchronization between the laser and electron beam by doing the position and the phase scans.

The search for the collisions area between the electrons and the laser photons has several degrees of freedom and is not straightforward. The two most sensitive degrees of freedom are the vertical position of the FPC (dimension orthogonal to the plane of the beams) and the relative phase between the laser and the electrons (time dimension). The search for collisions is performed in several steps:

- The FPC frequency is offset by at least 100 Hz with respect to the ATF frequency. By doing this the relative phase between the electrons and the laser is automatically scanned at a rate of at least 100 Hz.
- The vertical position of the FPC is swept slowly.
- While performing this vertical scan we look on the data acquisition oscilloscope for the apparition of short bursts in the output of the PMT (see figure 3). The length and the frequency of these bursts are related to the difference between the frequency of the cavity and the frequency of the ATF clock.
- Once these bursts have been found the vertical position of the laser is adjusted to maximize their intensity.
- At this stage the laser frequency can be locked on the ATF frequency.
- The phase of the laser with respect to the electron beam must be adjusted to optimize the intensity of the signal observed on the PMT output<sup>1</sup>.

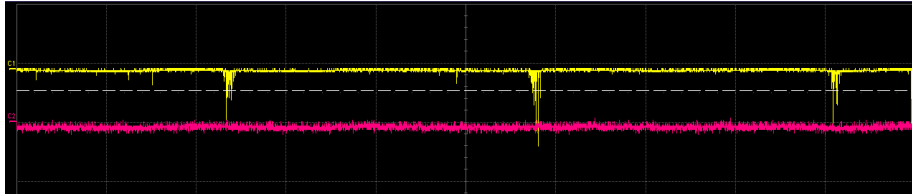


Figure 3: Example of signal observed on our oscilloscope while scanning the parameters space to find the collision area. The yellow line is the signal from the PMT. The duration of the waveform is 10 ms and the vertical scale is 200 mV (on this day the signal was amplified).

The bursts correspond to the time at which the phase of the laser matches that of the electrons. The distances between the bursts corresponds to the difference between the ATF frequency and the laser frequency. Each burst contains several peaks spaced by the duration of two DR revolution. The red line records the injection trigger (the trigger itself is off the screen). It was checked that the bursts on the yellow lines disappear when the cavity is moved vertically by a distance greater than the beam size.

#### 4.2 Example of data

During data taking we record the signal from the PMT as well as the 357 MHz ATF clock and the laser power transmitted by the FPC measured by a photodiode. To avoid the mistaking noise from the injection or extraction kickers a typical data acquisition starts at least 200 ms after the injection trigger is received. At this time we expect the beam to be almost fully damped. A typical signal waveform from the calorimeter can be observed on figure 4. A full waveform contains approximately 200 000 samples spaced by 1 ns.

<sup>1</sup>Our experience shows that the variation of this phase from day to day is small however we do observe small drifts which require a new phase scan on each run.

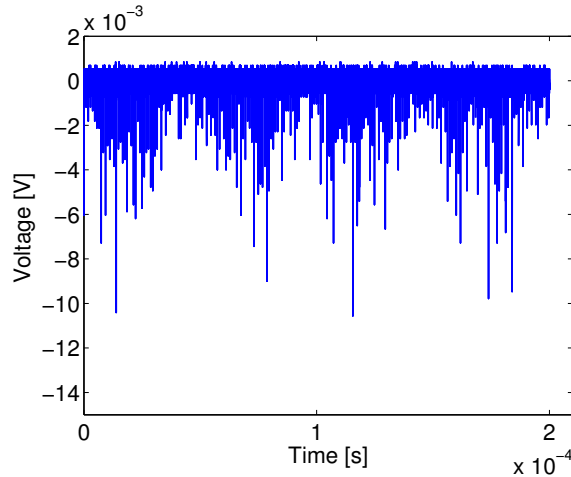


Figure 4: The typical signal shape for the high energy gamma rays produced by Compton scattering observed at the anode output of the PMT. Each spike on the picture corresponds to the gamma production after successive bunch crossings over 0.2 ms. Data shown correspond to a single bunch stored in the ATF DR.

### 4.3 Data analysis

The raw data recorded contain the intensity of the PMT output as a function of time (see figure 4). Data analysis was carried out to extract the intensity of the Compton signal and remove unwanted backgrounds.

As the data were acquired during the different ATF runs with different filling mode of the DR (1 train, 2 trains, 3 trains stored in the ATF DR) the correct number of Compton peaks and their timing must be found. The 357 MHz ATF clock is used to define the beginning of a 924 ns periods corresponding to the occurrence of the Compton signal (two ATF DR revolutions). All 924 ns periods belonging to one data file (usually 0.2 ms long) are superimposed on top of each other to find the number of the peaks per revolution and their time of arrival with respect to the beginning of the period. Such technique is used to enhance the signal over the background reducing at the same time the electronic noise. This results in a more precise way for the estimation of the number of the peaks and their timing. An example of stacking can be seen on figure 5a.

Once the number of peaks and their positions within the period is found we define a gate around the position where the Compton signal is expected. We use this gate to calculate the height and integral of the peak. The Compton peak height and its integral are our measure of the energy deposited by the gamma rays in the calorimeter. The length of the gate is set to 12 ns in order to entirely contain the signal thus ensuring a correct evaluation of the energy deposited. The distribution of such gates around the peak is presented on figure 5b.

The background level and its RMS are calculated within each period and are subtracted from the corresponding peak height and peak integral. The background level is defined as the mean over the timebase corresponding to a given period excluding the gate containing the signal. The average background level and its RMS for our data sample is estimated to be around  $7 \mu\text{V}$  and  $0.2 \text{ mV}$  respectively. Finally, the peak height and peak integral are calculated for every peak within the



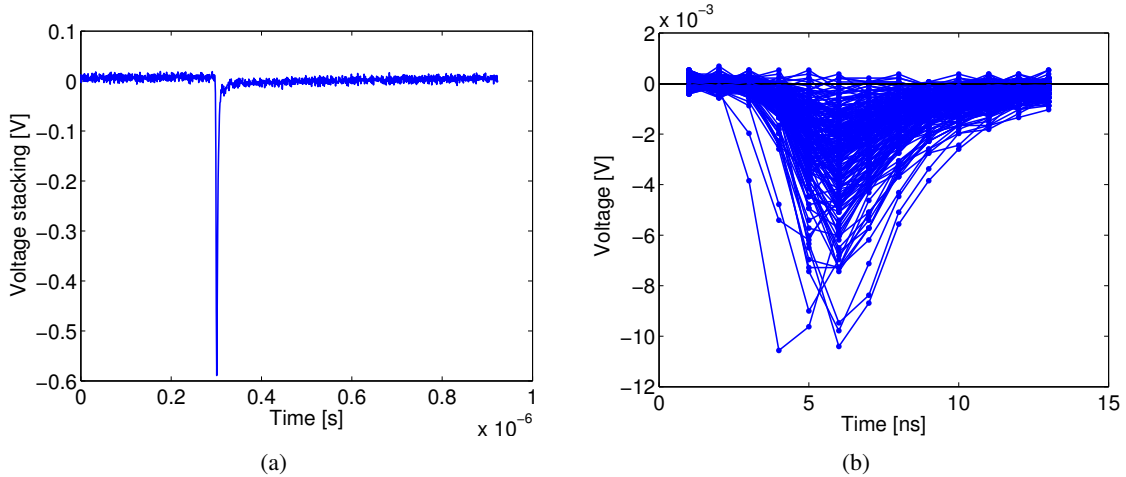


Figure 5: Stacking of all the 924 ns periods from the data file presented on figure 4 (figure 5a). This stacking is used to find the number of the peaks and their timing. Time profile of the signals for all the periods from the same file is shown on figure 5b.

period (see figure 6a).

The shape of the detector's response creates a linear relation between the total charge and the maximum charge measured. This can be seen as a correlation between the calculated peak height and peak integral as shown on figure 6b

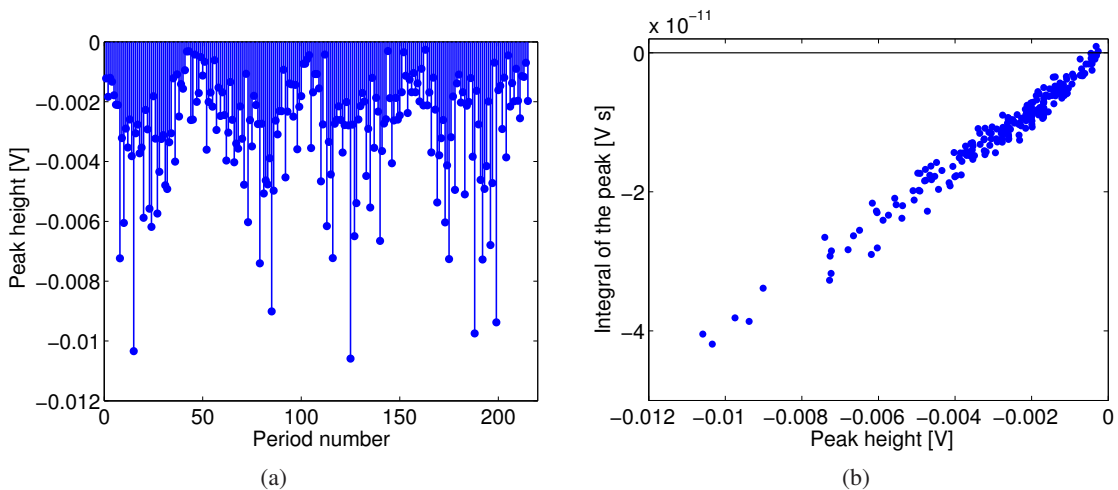


Figure 6: Figure 6a gives an example of the peak height distribution from the data file presented on figure 4. Peak height vs. peak integral for the same data file is shown on figure 6b.

**Quality of the data.** Different quality cuts are applied to restrict the analysis to a high purity sample. By putting limitations on them we can reject noise and obtain a set of good quality data (see figure 7).

We want all the Compton peaks within one file to have the same phase with respect to the ATF clock. It22 is achieved, in this case, by requiring the Compton signal to arrive 6 ns after the

beginning of the gate (see figure 7a).

Sometimes, the noise can dominate the signal (see figure 7b). Quite often, these signals can even lead to an integral value with the wrong sign. This is illustrated on figure 6b by the dots with positive values of the integral of the peak. Such events have to be considered as picked up noise and must be rejected. For this, we introduce a variable:

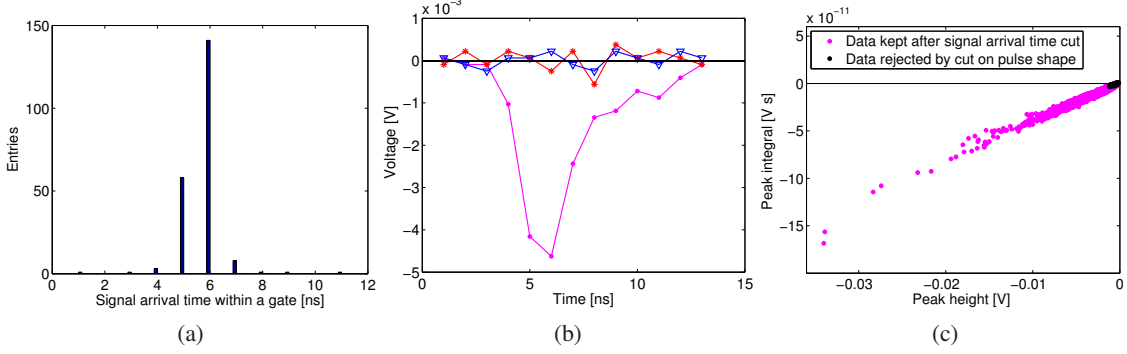


Figure 7: Quality cut illustration (figures 7a and 7b) shown together with their effect on all the data sample (figure 7c). Figure 7a: the distribution of the signal arrival time within the gate for all the signals found in the data file presented on figure 4. Figure 7b gives an example of a correct signal (magenta line) as opposed to the noise signal (blue, red line). Figure 7c shows the data sample remaining after the cut on the signal arrival time applied (magenta points) together with the events which are rejected due to the cut on the shape of the pulse (data points tagged in black).

$$V = \frac{2I_{max}(t_0)}{I(t_0 - 1) + I(t_0 + 1)}, \quad (4.1)$$

where  $I_{max}(t_0)$  is the intensity of the signal taken at the time when it reaches maximum,  $I(t_0 - 1)$  and  $I(t_0 + 1)$  are the intensities of the signal in the two nearest data points. By imposing  $1 \leq V \leq 10$  the noise is filtered out as  $V$  reaches either negative or very high positive values for noise signal. On figure 7b the magenta line corresponds to the real Compton signal for which our estimator variable  $V$  is about 1 while the red and blue lines are for the noise events and in this case  $V$  equals to -2 and 17 respectively.

The effect of the cuts mentioned above is shown on figure 7c. Cut on the signal arrival time preserve good linear relation between the peak height and peak integral apart from a few high intensity data points for which our data acquisition system saturated. The cut on the shape of the pulse helps to remove noise. However, some low intensity events still remain which correspond to the low energy deposited by the gamma rays in the calorimeter.

Approximately half of the data taken and presented in this study have been rejected after the different quality cuts have been applied. All the results commented below are based on high quality data sample.

**Background** While analysing the data we noticed that some data files contain peaks spaced by about 462 ns corresponding to one ATF DR revolution period. With the experimental setup we use

this is not possible because the electron bunch can not interact with laser pulses on two consecutive turns (see section 2). Such turn-by-turn background could be caused by the electrons hitting something inside the accelerator. To enforce high purity data, the files with such background are rejected.

**Laser power** On the day where the data presented in this article were taken, the average power stored in the FPC was approximately in average 160 W. It was measured by a photodiode placed behind one of the mirrors of the FPC and calibrated with a power-meter. Figure 8a shows the distribution of stored FPC laser power measured by the photodiode. As one can see, the FPC laser power experienced significant fluctuations which can be explained by several resonances in the FPC feedback system. Note that the feedback loop used to stabilize the laser power stored in the FPC had not yet been optimized at the time when these data were taken. On figure 8b the strong correlation between the laser power and the peak height distribution is clearly observed.

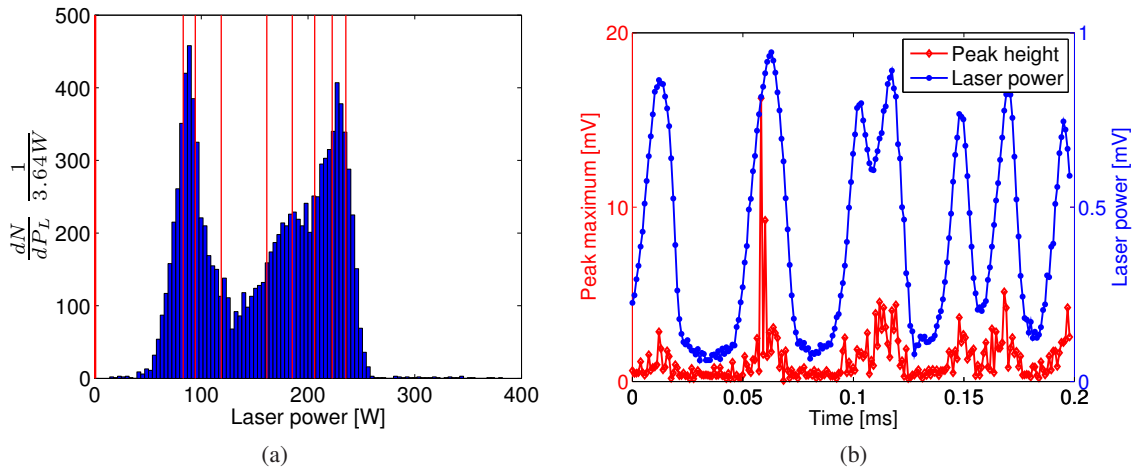


Figure 8: Figure 8a shows the histogram of the laser power stored in the FPC normalized by its maximum value. Red vertical lines divide the distribution into the nine laser power bins of approximately the same population each (see section 5). Figure 8b gives an example of the correlation between the transmitted FPC laser power and the gamma ray production intensity for a given data file. This can be seen by the correspondence between the peak height distribution (blue line) and the laser power measured by the photodiode at the same time (red line).

#### 4.4 Calibration

In the energy range (tens of MeV) of interest, the calorimeter can be calibrated by using cosmic rays muons. This calibration gives us a relation between the voltage measured on the oscilloscope and the energy deposited in the calorimeter.

In calibration mode the coincidences between two plastic scintillators, one placed at the top and the other at the bottom of the calorimeter, are used to trigger the data acquisition. The signal from the PMT is then digitized by the oscilloscope used to acquire the Compton data. Calibration measurements were performed before each data taking run. A typical measured distribution of pulse heights and pulse integrals is shown on figure 9.

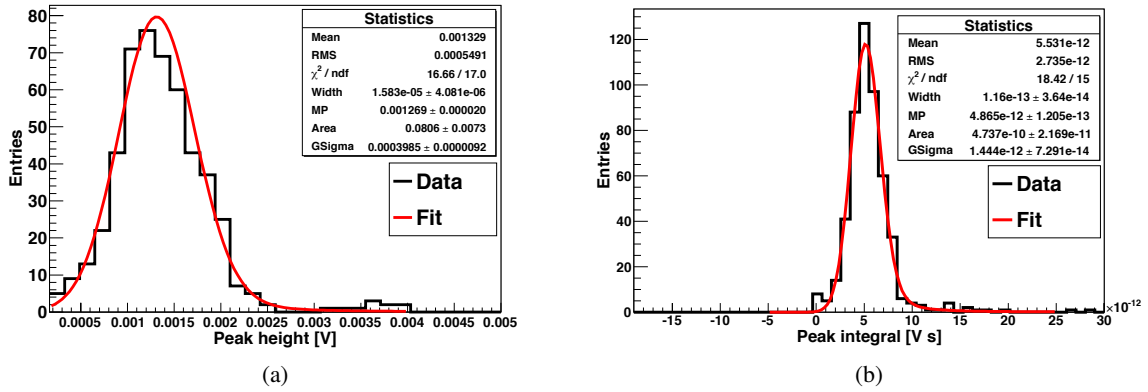


Figure 9: Energy loss distribution of the cosmic muons in the calorimeter. Figure 9a shows the histogram of the peak heights and figure 9b shows the histogram of the peak integrals. A Landau distribution fit with parameters is shown in both cases.

For detectors of moderate thickness such as the one we are using, the energy loss probability distribution is described by the Landau distribution [23]. The most probable energy loss of cosmic muons is the most probable value (MPV) of the Landau distribution.

According to our calibration, the MPV for the integrated signal is  $(4.87 \pm 0.12)$  mV·ns and the MPV for the peak height distribution is  $(1.27 \pm 0.02)$  mV. Assuming minimum ionization, the energy deposition in the calorimeter is 6.374 MeV/cm [24]. This value corresponds to approximately 45 MeV of energy deposited by a muon passing through the calorimeter. However, this value should be corrected to account for the geometry and the acceptance of the detection system.

To do so, the measure should be scaled by the ratio between the total number of optical photons produced in the  $BaF_2$  crystal and those optical photons which are within the PMT acceptance. Another correction factor appears due to the fact that the two surrounding plastic scintillators are not fully covering the surface of the  $BaF_2$  crystal. Therefore, the previous factor has to be corrected to take into account this difference in overlapping surfaces. To address these two issues we used a Geant4 simulation of the detector which gave a correction factor of  $0.745 \pm 0.001(\text{stat}) \pm 0.04(\text{sys})$ .

Once, all corrections have been applied, a peak height of 1 mV and peak integral of 1 mV·ns is equivalent in average to  $(26.6 \pm 1.9)$  MeV and  $(6.9 \pm 0.5)$  MeV of energy deposited in the calorimeter respectively.

## 5. Results

The data analysis performed in this study were done to evaluate the number of gamma rays produced during the collisions between the electrons and laser photons.

The spectrum of the gamma rays is shown on figure 10a and 10b. It represents the distribution of the energy deposited in the calorimeter expressed by the peak integrals<sup>2</sup>.

Using our calibration, we can estimate the average number of scattered gammas per bunch crossing. As it was shown in section 3, the mean energy of scattered gammas we measure is

<sup>2</sup>The similar spectra could be obtained by using the Compton peak height as a measure of energy deposited in the calorimeter.

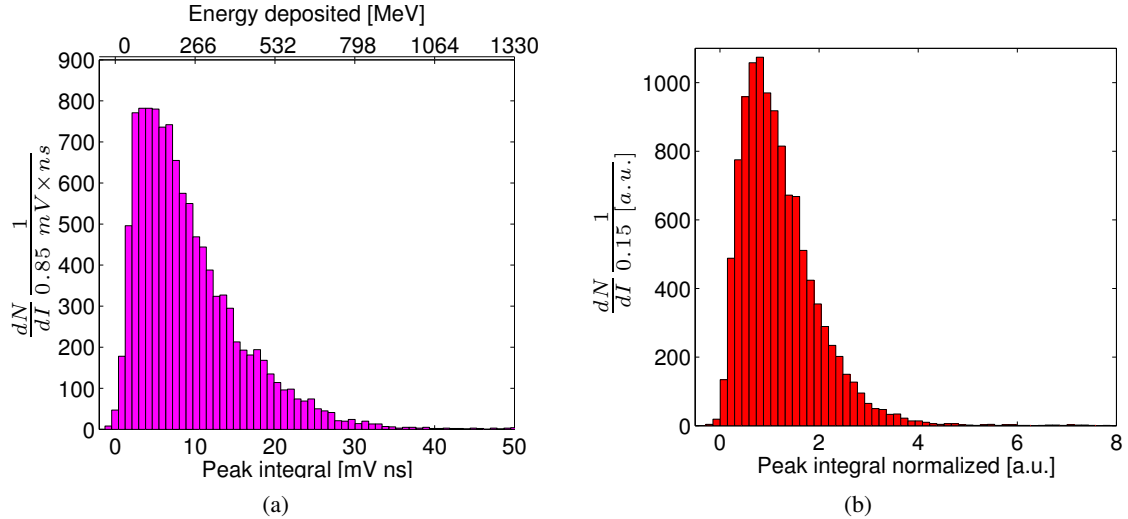


Figure 10: Spectrum of the gamma rays produced for all laser powers. Figure 10a shows the distribution of the integrals of the Compton peaks for the high quality data sample whereas the figure 10b shows the same spectrum normalized by the laser power.

24 MeV. Since the average energy deposited per bunch crossing is  $65.1 \pm 4.9$  MeV, we deduce that approximately  $2.7 \pm 0.2$  gammas are produced in average per bunch crossing (for an average laser power stored in the FPC of about 160 W). This rate of about 2.7 gammas per bunch crossing was successfully sustained over 6 hours until the end of our run. For the given collision repetition frequency in the ATF DR of about 1 MHz, the flux of gamma rays achieved is about  $3 \times 10^6$  gammas per second (this does not take into account the 0.75 duty cycle of the ATF).

To verify the linearity of the gamma ray flux as a function of the laser power stored in the FPC, we took data over a wide range of laser power (see subsection 4.3). The laser power distribution has been split into the nine bins of approximately 1300 events each as it is shown on figure 8a. Then, the gamma production has been studied within each laser power bin. The spectra of scattered gamma rays which correspond to the different values of laser power stored in the FPC are presented on figure 11a. As expected, the average of the peak integral distribution (energy deposited in the calorimeter by the gamma rays) scales linearly with the laser power stored in the FPC (see figure 11b).

**Data - simulations comparison** Simulations were carried out to have a comparison with the gamma ray spectrum obtained experimentally. Noise was introduced in the simulations and quality cuts were applied in the same manner for both data and simulations.

The spectrum of gamma rays measured is shown on figure 12 together with the spectrum simulated for a MPV of 2.7 gammas. The spectrum corresponds to the distribution of the energy deposited in the calorimeter expressed by the peak heights.

Figure 12 shows a very good agreement between the experimental data and simulations.

**Highest integrated/instantaneous flux** We scanned our data for the best integrated and instantaneous gamma flux which was produced. The best instantaneous flux we measured (the highest energy deposition) was 34 mV which according to the calibration corresponds to  $904 \pm 65$  MeV

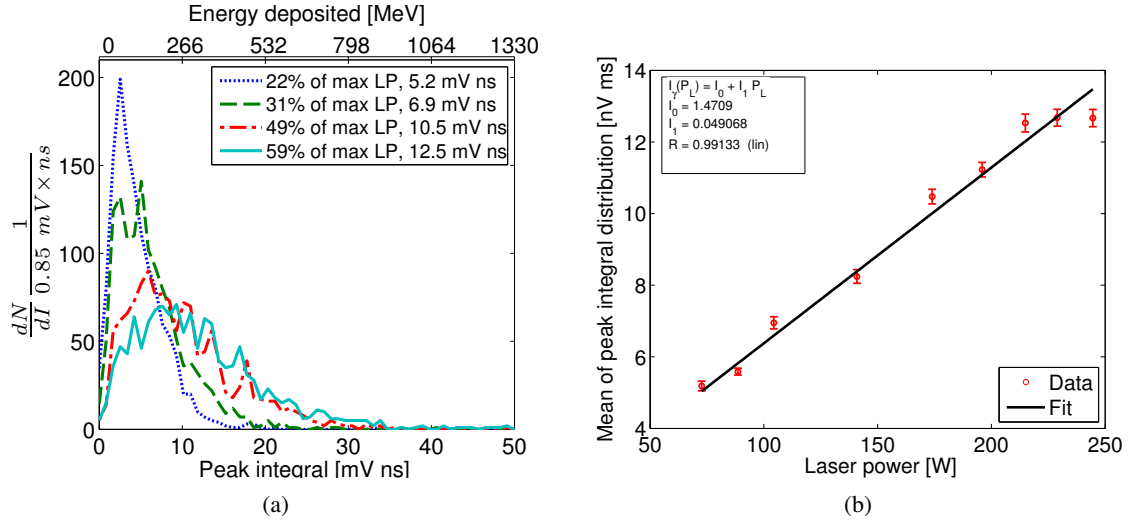


Figure 11: Figure 11a presents gamma spectrum for different FPC stored laser power. Different colors correspond to the spectra taken at different FPC powers. In the legend, the fraction of the maximum FPC stored power and the mean of each of these spectra are shown. Figure 11b shows the linear relation between the mean of gamma spectra for each laser power bin and the correspondent laser power which is defined as a mean of the laser power bins shown on figure 8a. The errors bars indicate the statistical errors.

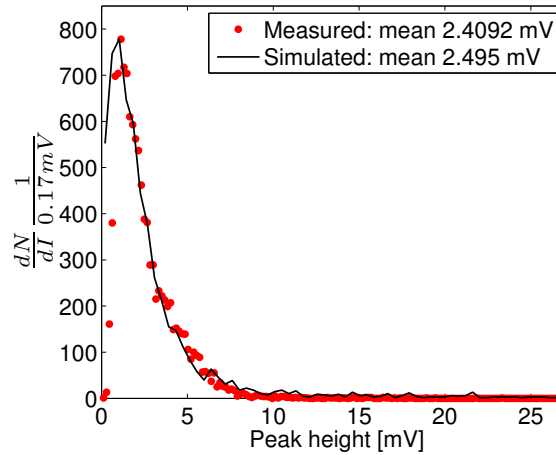


Figure 12: Comparison between the measured and simulated energy spectra of the gamma rays resulting from Compton scattering. The black solid line represents the simulated spectrum and the circles dots represent the measured gamma ray energy distribution expressed in the peak heights. For the simulations the events occur according to a Poisson process with a rate of 2.7 gammas per bunch crossing. The data presented are the same than those of figure 10a.

deposited in the calorimeter. Assuming 24 MeV per gamma, this gives about  $38 \pm 3$  gammas produced per bunch crossing. The corresponding Compton peak can be seen on figure 13.

For the many applications of accelerator driven Compton sources an important characteristic

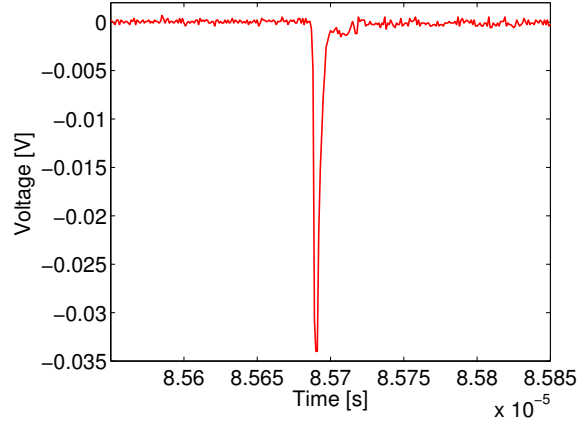


Figure 13: Part of the data file containing the highest energy deposited in the calorimeter per one shot which is about 904 MeV. Waveform shows this event which stands for the highest instantaneous gamma flux we measured. It is equivalent to 38 gammas produced in one bunch crossing.

is the total gamma flux. Table 3 summarizes the results concerning the highest gamma ray flux integrated over 0.2 ms (duration of one data file) for different ATF DR filling modes. As one can see, the total flux does not scale linearly with the number of electron bunches stored in the DR contrary to what was expected. Additional studies should be conducted to investigate this issue. Figure 14 shows the three data files having the best integrated gamma ray flux.

Table 3: Highest integrated gamma ray flux achieved.

Electron pulse structure	Total intensity over 0.2 ms	Energy deposited over 0.2 ms	Integrated flux over 0.2 ms	Integrated flux over 1 s	Systematic error
1 train	893 mV	23750 MeV	990 $\gamma$	$\sim 4.9 \times 10^6 \gamma$	7%
2 trains	910 mV	24210 MeV	1010 $\gamma$	$\sim 5.0 \times 10^6 \gamma$	7%
3 trains	1010 mV	26800 MeV	1120 $\gamma$	$\sim 5.6 \times 10^6 \gamma$	7%

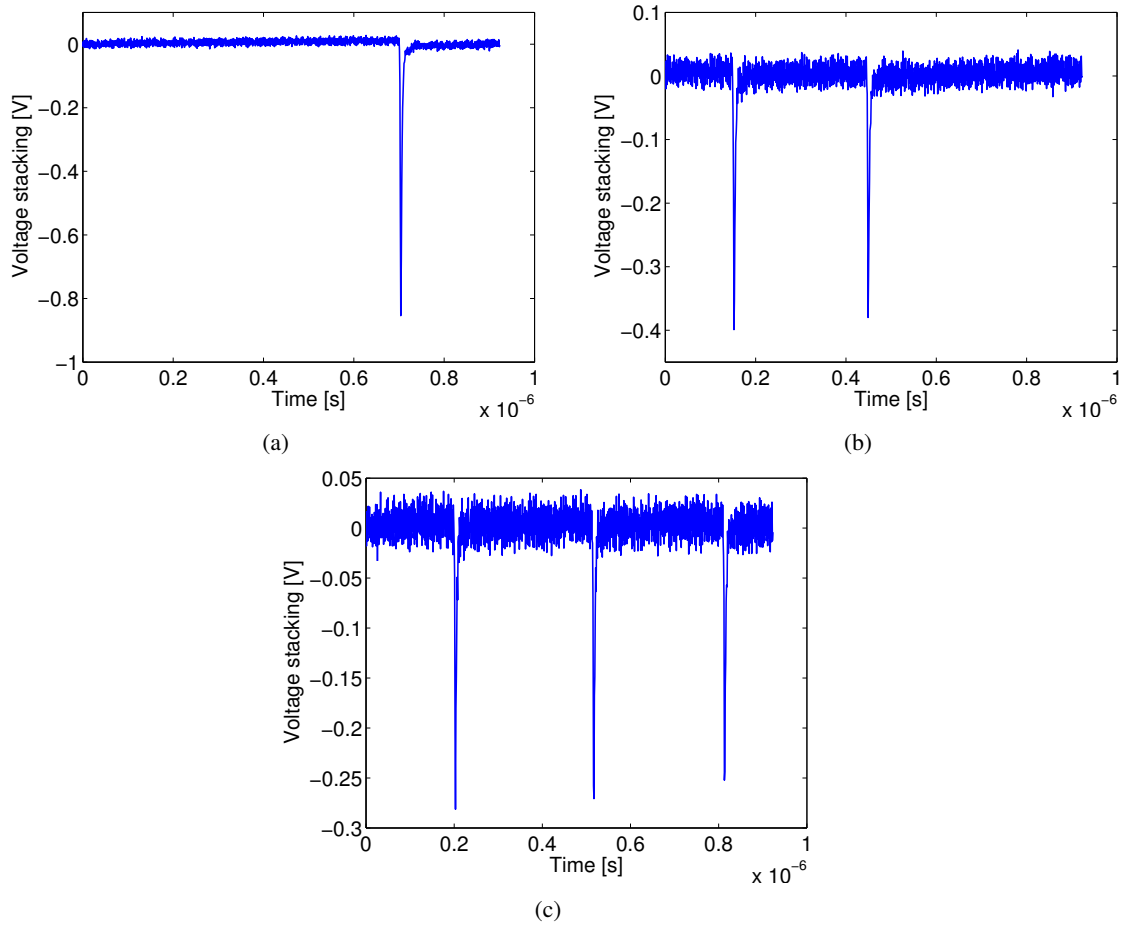


Figure 14: Illustration of three data files containing the highest integrated flux over 0.2 ms for different ATF DR filling modes: one bunch stored in the DR (figure 14a), two trains of one bunch each stored in the DR (figure 14b) and three trains of one bunch each stored in the DR (figure 14c). The figures show all the periods of a given file stacked together.

## 6. Conclusion and outlook

The MightyLaser project has demonstrated the production of gamma rays using a non-planar four-mirror FPC. In average,  $2.7 \pm 0.2$  gammas are produced per bunch crossing. This result is in agreement with the CAIN simulations for the FPC laser power achieved in the experiment. A good agreement is also observed between the measured and simulated energy spectra of the gamma rays using Geant4 toolkit. The highest integrated flux of  $1120 \pm 80$  gammas over 0.2 ms ( $\sim 5.6 \times 10^6$  gammas per second) in three trains mode and an instantaneous flux of  $38 \pm 3$  gammas per bunch crossing were measured. These values are limited by the FPC laser power obtained so far.

Work to improve the laser stability and increase the FPC finesse has been interrupted by the earthquake which hit Japan in March 2011. Operation of the ATF at KEK is to be resumed soon. Our objective for the next campaign is to increase production of high energy gamma rays by several orders of magnitude by increasing both the FPC finesse and the input laser power.



## Acknowledgements

This work has been funded by the French ANR (Agence Nationale de la Recherche) contract number BLAN08-1-382932 and P2I (Physique des 2 Infinis). The authors would like to thank the staff from KEK for their hospitality.

## References

- [1] J. Bonis et al. Non-planar four-mirror optical cavity for high intensity gamma ray flux production by pulsed laser beam Compton scattering off GeV-electrons. *To be submitted to JINST*.
- [2] S. Araki et al. Design of a polarised positron source based on laser Compton scattering. *Arxiv preprint physics/0509016*, 2005.
- [3] M. Kuriki et al. ILC positron source based on laser Compton. *AIP Conf.Proc.*, 980:92–101, 2008.
- [4] O. Dadoun et al. The Baseline Positron Production and Capture Scheme for CLIC. 1st International Particle Accelerator Conference: IPAC'10, 23-28 May 2010, Kyoto, Japan.
- [5] P. Walter et al. A new high quality x-ray source for cultural heritage. *Comptes Rendus Physique*, 10(7):676 – 690, 2009.
- [6] ThomX collaboration. Thomx CDR. *IN2P3*, in2p3-00448278, 2010.
- [7] A. Loulergue et al. A Compact Ring for the ThomX-ray Source. 1st International Particle Accelerator Conference: IPAC'10, 23-28 May 2010, Kyoto, Japan.
- [8] J. Urakawa. Development of a compact x-ray source based on Compton scattering using a 1.3 GHz superconducting RF accelerating linac and a new laser storage cavity. *Nuclear Instruments and Methods in Physics Research Section A: Accelerators, Spectrometers, Detectors and Associated Equipment*, 2010.
- [9] P. Sprangle et al. Tunable, short pulse hard x-rays from compact laser synchrotron source. *Appl. Phys.*, 72:5032–5034, 1992.
- [10] H. Kogelnick and T. Li. Laser beams and resonators. *Appl. Opt.*, 5:1550–1567, 1966.
- [11] Z. Huang and R. D. Ruth. Laser-electron storage ring. *Phys. Rev. Lett.*, 80(5):976–979, Feb 1998.
- [12] F. Hinode et al. ATF accelerator test facility design and study report No. 4. KEK, Tsukuba, Japan, 1995. <http://lcdev.kek.jp/ATF/Pub/KEK-I-95-4.pdf>.
- [13] H. Shimizu et al. Photon generation by laser-Compton scattering using an optical resonant cavity at the KEK-ATF electron ring. *Journal of the Physical Society of Japan*, 78(7):4501, 2009.
- [14] S. Miyoshi et al. Photon generation by laser-Compton scattering at the KEK-ATF. *Nuclear Instruments and Methods in Physics Research Section A: Accelerators, Spectrometers, Detectors and Associated Equipment*, 2010.
- [15] H. Hayano et al. Accelerator test facility study report JFY 19996-1999. *KEK, Tsukuba, Japan*, KEK Internal report 2000-6, 2000.
- [16] P. Bambade et al. Present status and first results of the final focus beam line at the KEK Accelerator Test Facility. *Phys. Rev. ST Accel. Beams*, 13(4):042801, Apr 2010.
- [17] T. Naito et al. Timing system for multi-bunch/multi-train operation at ATF-DR. *KEK, Tsukuba, Japan*, KEK Preprint 99-144, 1999.

- [18] S. Miyoshi. *Development of polarized positron source by laser Compton scattering with optical resonant cavity*. PhD thesis, Graduate School of Advanced Sciences of Matter, Hiroshima University, 2011.
- [19] S. Agostinelli et al. Geant4: A simulation toolkit. *Nucl. Instrum. Meth.*, A506:250–303, 2003.
- [20] K. Yokoya. User manual of CAIN, version 2.40, 2009.
- [21] T. Suzuki. General formulae of luminosity for various types of colliding beam machines. *KEK note*, pages 76–3.
- [22] V. B. Berestetskii, L. D. Landau, E. M. Lifshitz, L. P. Pitaevskii, J. B. Sykes, and J. S. Bell. *Quantum electrodynamics*, volume 4. Butterworth-Heinemann, 1982.
- [23] L. Landau. On the energy loss of fast particles by ionisation. *J. Phys. USSR*, 8(4):201, 1944.
- [24] D. Groom. Atomic and nuclear properties of materials. Particle Data Book.  
<http://pdg.lbl.gov/2011/AtomicNuclearProperties/>.